J Therm Anal Calorim (2010) 101:987–996
DOI 10.1007/s10973-009-0560-z

Thermal behaviour and spectroscopic studies of complexes of some divalent transitional metals with 2-benzoil-pyridil-izonicotinoylhydrazone

Lucica Viorica Ababei · Angela Kriza · Adina Magdalena Musuc · Cristian Andronescu · Elena Adina Rogozea

Received: 5 September 2009 / Accepted: 13 October 2009 / Published online: 5 November 2009

Abstract New complexes of 2-benzoyl-pyridil-isonicotinoylhydrazone (L) with Cu(II), Co(II), Ni(II) and Mn(II), having formula of type $[ML_2]\,SO_4{\cdot}xH_2O$ ($M = Cu^{2+}, Co^{2+}, Ni^{2+}, x = 2$ and $M = Mn^{2+}, x = 3$), have been synthesised and characterised. All complexes were characterised on the basis of elemental analyses, IR spectroscopy, UV–VIS–NIR, EPR, as well as thermal analysis and determination of molar conductivity and magnetic moments. The thermal behaviour of complexes was studied using thermogravimetry (TG), differential thermal analysis (DTA) and differential scanning calorimetry (DSC). The structure of L hydrazone was established by X-ray study on single crystal. The ligand works as tridentate NNO, being coordinated through the azomethine nitrogen, the pyridine nitrogen and carbonylic oxygen. Heats of decomposition, ΔH, associated with the exothermal effects were also determined.

Keywords 2-Benzoyl-pyridil-isonicotinoylhydrazone · Template synthesis · Transition metal complexes · Thermal analysis · X-ray study

L. V. Ababei (✉)
The House of Teaching Staff Giurgiu, 8, Nicholae Droc Barcian Street, Giurgiu, Romania
e-mail: lucica_32@yahoo.com

A. Kriza
Faculty of Chemistry, University of Bucharest, 23 Dumbrava Rosie Street, Bucharest, Romania

A. M. Musuc · C. Andronescu · E. A. Rogozea
Romanian Academy, "Ilie Murgulescu" Institute of Physical Chemistry, 202 Independence Avenue, 060021 Bucharest, Romania

Introduction

The coordination chemistry of Schiff base ligands derived from 2-pyridyl ketones has received more and more attention. In 1990, Gourbatsis et al. [1] found a rich and varied coordination chemistry of Schiff base ligands derived from 2-acetylpyridine and 2-benzoylpyridine. Particularly, tridentate ONO/S, NNO/S and PNO/S functionalised ligands have recently attracted considerable interest [2–6], but surprisingly NNO-chelating ligands have been little published [7–9]. The tautomerism of these ligands as well as the well-known transition metal chelating properties allows various structural possibilities [10] for its metal complexes. In addition, the versatile applications of Schiff base ligand complexes in the field of biological [11–13] and industrial processes [14, 15] prompted us to synthesise the tridentate NNO-Schiff base ligand complexes [16, 17].

The thermal analysis techniques such as thermogravimetry (TG), differential thermal analysis (DTA) and differential scanning calorimetry (DSC) were widely applied in studying of the thermal behaviour of metal complexes [18–20]. The data provided information concerning the thermal stability and thermal decomposition of these compounds in the solid state.

In the context of our previous research, a number of four complexes of transition metals with ligand derived from 2-acetylpyridine [21] and 2-benzoylpyridine [22] were obtained and characterised.

In the present paper, we report synthesis and characterisation of four combinations of Cu(II), Co(II), Ni(II) and Mn(II) sulphate with 2-benzoyl-pyridil-isonicotinoylhydrazone (L). The structural ligand formula is shown in Fig. 1.

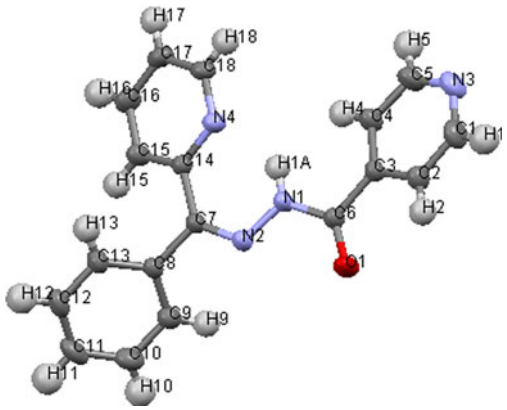

Fig. 1 The crystal structure of 2-benzoyl-pyrydil-isonicotinoylhydrazone (L)

Experimental

Materials

All chemicals were of pure analytical grade and were purchased from Sigma-Aldrich and Fluka.

Synthesis of 2-benzoyl-pyridil-isonicotinoylhydrazone

The 2-benzoyl-pyridil-isonicotinoylhydrazone—L was obtained by refluxing on water bath for 5 h, a mixture of isoniazid and 2-benzoyl-pyridine (ratio 1:1 molar). Methanol (30 mL) was used as a solvent. After cooling, a pink precipitate occurs. This is filtered, washed with methanol and dried in vacuum on $CaCl_2$. The solid was separated from single crystals and the X-ray crystal structure has been made.

Synthesis of complexes

A methanolic solution of isoniazid (0.002 moles in 30 mL of methanol) is added to the methanolic solution of 2-benzoyl-pyridine (0.002 moles in 30 mL methanol). The mixture was stirred at 50 °C for 30 min, cooled at room temperature and to this was added under stirring, the methanolic solution of Cu(II), Co (II), Ni(II) and Mn(II) sulphate (0.001 moles in 15 mL methanol). Immediately, the metallic complexes are precipitates. The solid products (1–4) are filtered, washed with methanol and dried in vacuum over anhydrous $CaCl_2$.

Techniques

The elemental analyses (C, H, N) were made with an Elemental Combustion System CHNS-O, using a Costech device, type ECS 4010, and the metal content was determined by gravimetric methods: Cu with salicylaldoxime, Ni with dimethilglioxime, and Co and Mn as pyrophosphates.

The melting temperatures of complexes were directly measured with SMPI Melting Point Apparatus (Stuart Scientific). Molar conductances of the complexes were measured in 10^{-3}M DMF at room temperature using a Consort type C-533 conductivity instrument.

The IR spectra (4000–400 cm^{-1}) were recorded in KBr tablet, using a BIO-RAD FTS-135 spectrometer, and the UV–Vis–NIR electronic spectra (200–2200 nm) were recorded with a UV–Vis–NIR spectrophotometer in diffuse reflectance, JASCO V 670.

The measurements of magnetic susceptibility were determined at room temperature, using the Faraday method, and electronic paramagnetic resonance (EPR) spectra of Cu(II) complex were recorded at room temperature, on a Jeol JESS FA 100 spectrometer, with a 100 Hz field modulation.

The thermal experiments were performed on a Mettler Toledo TGA/SDTA 851^e thermal analyzer, within the temperature range 25–1000 °C, and a Mettler Toledo DSC 853^e differential scanning calorimeter, within the temperature range 25–600 °C. The TG curves were recorded in nitrogen atmosphere with a flow rate of 50 mL min^{-1} and at a heating rate of 5 K min^{-1}. The DSC curves were obtained under nitrogen atmosphere with 80 mL min^{-1} flow rate and a 10 K min^{-1} heating rate. The samples were held in aluminium crucibles for DSC experiments and platinum crucibles for TG/SDTA experiments, with a pinhole in the lid to prevent pressure build up due to gaseous products. Sample mass was between 0.8 and 3 mg for both methods. At the end of the heating process for the DSC experiments, the mass of the remaining sample represents approximately 30% from initial values for all studied complexes. The TG/DTA and DSC curves were used to characterise the accompanying mass and heat changes during the linear heating.

Single-crystal X-ray diffraction was used for crystal structure determination of 2-benzoyl-pyridil-isonicotinoylhydrazone. XRD data were collected on a STOE IPDS II diffractometer operating with a Mo Kα ($\lambda = 0.71073$ Å) X-ray tube with a graphite monochromator, at room temperature. Data collection: Stoe X-AREA [23]. Cell refinement: Stoe X-AREA [23]. The structures were solved by direct methods and refined with anisotropic displacement parameters based on F^2, using SHELXS-97 [24] and SHELXL-97 [25] crystallographic software packages.

Results and discussion

The structure of L (L = 2-benzoyl-pyridil-isonicotinoylhydrazone) was determined using X-ray study on single crystal.

Table 1 Crystallographic data, details of data collection and structure refinement parameters for ligand (L)

Chemical formula	$C_{18}H_{14}N_4O_1$
M/g mol^{-1}	302.33
Temperature/K	293(2)
Wavelength/Å	0.71073
Crystal system	Triclinic
Space group	*P*-1
a/Å	8.317(1)
b/Å	8.683(1)
c/Å	11.079(1)
α/°	91.599(1)
β/°	93.941(1)
γ/°	109.486(1)
V/Å^3	751.38(2)
Z	2
F(000)	316
Reflections collected	5693
Unique reflections	4212
Goodness-of-fit on F^2	1.050

Details of crystal structure determination are summarised in Table 1, and bond lengths and the angles are collected in Table 2.

Complexes with L are obtained by template synthesis. The compounds are soluble in DMF and insoluble in other common organic solvents (methanol, ethanol, acetone, diethyl ether, chloroform). Molar conductivity measurements in DMF show that they are 1:1 type electrolytes [26].

Elemental analysis is shown in Table 3. The analytical data show that the complexes may be formulated as $[ML_2](SO_4)\cdot xH_2O$, where M = Cu(II), Co(II), Ni(II), $x = 2$ and M = Mn(II), $x = 3$, L = 2-benzoyl-pyridil-isonicotinoyl-hydrazone.

Some physical properties (colour, melting point, molar conductivity in DMF 10^{-3} M) of the complexes are given in Table 3.

Infrared spectra

The main bands from IR spectra of ligand (L) and its metal complexes are presented in Table 4.

In the 2-benzoyl-pyridil-isonicotinoylhydrazone (L) IR spectra, a very intensive band appears at 1691 cm^{-1} and a strong band appears at 1668 cm^{-1}, which are assigned to the vibration frequency *ν*(C=O) amide I [27] and *ν*(C=N) azomethine [28].

For complexes 1–4, the band group corresponding to amide I appear shifted with 29–38 cm^{-1} towards lower frequencies, which indicates the involvement of carbonyl group in coordination [29]. Also, a shift towards lower

Table 2 Bond distances and angles for ligand (L)

Bond lengths
C1–N3 1.333(2)
C1–C2 1.3832(2)
C2–C3 1.3875(2)
C3–C4 1.3873(2)
C3–C6 1.5053(1)
C4–C5 1.3887(2)
C5–N3 1.332(2)
C6–O1 1.2156(1)
C6–N1 1.3601(1)
C7–N2 1.2961(1)
C7–C14 1.4904(15)
C7–C8 1.4953(1)
C8–C13 1.3913(2)
C8–C9 1.3913(2)
C9–C10 1.3897(2)
C10–C11 1.382(2)
C11–C12 1.377(2)
C12–C13 1.3892(2)
C14–N4 1.3506(1)
C14–C15 1.3913(2)
C15–C16 1.3851(2)
C16–C17 1.3790(2)
C17–C18 1.3784(2)
C18–N4 1.3380(15)
N1–N2 1.3678(1)
Bond angles
N3–C1–C2 124.16(1)
C1–C2–C3 118.79(1)
C4–C3–C2 117.81(1)
C4–C3–C6 124.20(1)
C2–C3–C6 117.99(1)
C3–C4–C5 118.82(1)
N3–C5–C4 123.88(1)
O1–C6–N1 124.84(1)
O1–C6–C3 121.89(1)
N1–C6–C3 113.26(9)
N2–C7–C14 127.53(9)
N2–C7–C8 114.49(9)
C14–C7–C8 117.92(9)
C13–C8–C9 118.91(1)
C13–C8–C7 121.27(1)
C9–C8–C7 119.82(1)
C10–C9–C8 120.36(1)
C11–C10–C9 120.12(1)
C12–C11–C10 119.92(1)
C11–C12–C13 120.29(1)
C12–C13–C8 120.35(1)
N4–C14–C15 120.97(1)
N4–C14–C7 118.05(9)

Table 2 continued

C15–C14–C7 120.94(1)
C16–C15–C14 119.42(1)
C17–C16–C15 119.53(1)
C18–C17–C16 117.86(1)
N4–C18–C17 123.68(11
C6–N1–N2 120.29(9)
C7–N2–N1 117.83(9)
C5–N3–C1 116.50(1)
C18–N4–C14 118.54(1)

values of $\Delta\nu = 66$–$77\ cm^{-1}$ is observed for the frequencies characteristic to azomethine group of metal complexes with 2-benzoyl-pyridil-isonicotinoylhydrazone. This suggests the involvement of azomethine nitrogen in coordination with metallic ions [29].

In the IR spectra of the ligand, three mid intensity bands appear at 1548, 1000 and 743 cm^{-1}, which are assigned to vibration frequency ν(Py ring), Py ring bending and γ (Py ring outside the plan), respectively.

In complexes 1–4, vibration frequency due to the Py ring is displaced to lower values. On the other hand, in the IR spectra of complexes the band corresponding the Py ring bending, which in ligand is at 1000 cm^{-1}, is displaced to higher values, with $\Delta\nu = 16$–$57\ cm^{-1}$. Displacements to higher values with $\Delta\gamma = 12$–$14\ cm^{-1}$ also appear for the typical band of γ (Py ring outside the plan).

This information leads to the idea that pyridine nitrogen of 2-benzoyl pyridine is involved in the coordination with metal ions [30, 31]. All data support the idea that in the metallic complexes, the ligand works as tridentate NNO, being coordinated through the azomethine nitrogen, the pyridine nitrogen and carbonylic oxygen.

The IR spectra of complexes 1–4 also show the band attributed to the counteranion SO_4^{2-} [29].

Magnetic moments

The magnetic moments for all complexes were determined at room temperature, using the diamagnetic correction [32] (Eq. 1):

$$\chi_D = kM * 10^{-6}\ cm^3\ mol^{-1} \quad (1)$$

where M is the molecular weight of the compound and k a factor varying between 0.4 and 0.5.

The magnetic moment calculated for Cu(II) complex is 2.09 B.M. This value reasonably corresponds to the octahedral geometry of Cu(II) complexes [33].

For the Co(II) complex, the magnetic moment experimentally determined is 4.68 B.M., indicating a high-spin character and excluding the oxidation to Co(III). This value is within the range (4.3–5.7 B.M.), corresponding to an octahedral geometry for cobalt ion [33].

For the Ni(II) complex, the value of the magnetic moment is 2.98 B.M. This is within the range (2.8–3.5 B.M.) found for the paramagnetic Ni(II) complexes with an octahedral geometry [33].

The magnetic moment determined for the Mn(II) complex is 5.65 B.M. This value falls in the range 5.65–6.10

Table 3 Analytical and physical data of the complexes

Compounds	Colour	Melting point/°C	$\Lambda^*/\Omega^{-1}\ cm^2\ mol^{-1}$	$\mu_{eff/BM}$	Elemental analysis found (Calcd.)			
					M/%	C/%	H/%	N/%
$[CuL_2]SO_4{\cdot}2H_2O$ (1)	Green turquoise	235	98.2	2.09	7.764 (7.945)	54.231 (54.013)	4.364 (4.033)	14.117 (14.003)
$[CoL_2]SO_4{\cdot}2H_2O$ (2)	Pink	>325	117	4.68	7.543 (7.411)	54.675 (54.327)	4.330 (4.056)	14.101 (14.084)
$[NiL_2]SO_4{\cdot}2H_2O$ (3)	Blue	298**	111	2.98	7.67 (7.39)	54.665 (54.395)	4.322 (4.061)	14.233 (14.102)
$[MnL_2]SO_4{\cdot}3H_2O$ (4)	White	>325	98.1	5.65	6.559 (6.789)	53.200 (53.385)	3.687 (3.986)	13.471 (13.840)

* DMF solution 10^{-3} M at 20 °C

** With decomposition

Table 4 Selected infrared absorption frequencies (cm^{-1}) of L and complexes

Compounds	ν(OH)	νN–H	νC=O amide I	νC=N azomethine	ν(Py ring)	νSO_4^{2-}	Py ring bending	γ (Py ring outside the plan)
L	–	3303 3110	1691	1668	1548	–	1000	743
$[CuL_2]SO_4{\cdot}2H_2O$	3420	3117 3086	1653	1591	1540	1146–1117	1041	756
$[CoL_2]SO_4{\cdot}2H_2O$	3400	3279 3100	1655	1595	1548	1143–1093	1057	755
$[NiL_2]SO_4{\cdot}2H_2O$	3400	3246 3081	1658	1603	1551	1107	1087	756
$[MnL_2]SO_4{\cdot}3H_2O$	3400	3281 3094	1662	1602	1547	1117	1016	757

B.M. and it is appropriate to the manganese ion, with an octahedral environment [34].

Electronic spectra

The Schiff base (L) presents in UV spectra two bands at 37593 and 32679 cm^{-1}, assigned to $\pi \rightarrow \pi^*$ and $n \rightarrow \pi^*$ transitions.

The electronic spectrum of the Cu(II) complex, presents a large band at 12722 cm^{-1}, which can be attributed to the xz, $yz \rightarrow x^2 - y^2$ transition, proper for an octahedral geometry [35].

The electronic spectra of Co(II) complex presents three bands at 8532, 5337 and 19455 cm^{-1}, attributed to the d–d transitions $^4T_{1g} \rightarrow {}^4T_{2g}$, $^4T_{1g}(F) \rightarrow {}^4A_{2g}$ and $^4T_{1g} \rightarrow {}^4T_{1g}(P)$, respectively. These transitions and the values of the field parameters correspond to those characteristic for an octahedral geometry [35].

The electronic spectrum of Ni(II) complex (Fig. 2) presents three bands, at 9708, 16025 and 25906 cm^{-1}, attributed to the $^3A_{2g} \rightarrow {}^3T_{2g}$, $^3A_{2g} \rightarrow {}^3T_{1g}$ and, respectively, $^3A_{2g} \rightarrow {}^3T_{1g}$ (P) transitions, proper to an octahedral geometry for the nickel ion [35].

The ligand field splitting energy ($10\Delta q$), interelectronic repulsion parameter (B) and nephelauxetic ratio (β) for the Co(II) and Ni(II) complexes were calculated using the secular equations given by König [36] and the values are presented in Table 5.

The Mn(II) complex presents a signal in UV domain at 30862 cm^{-1} assigned to a transfer of electric load, according with the theory data for a d^5 ion. It is well-known that the d–d transitions occur in the d^5 systems but those transitions are of very low intensities and hence we did not observe any d–d bands for such transitions [34].

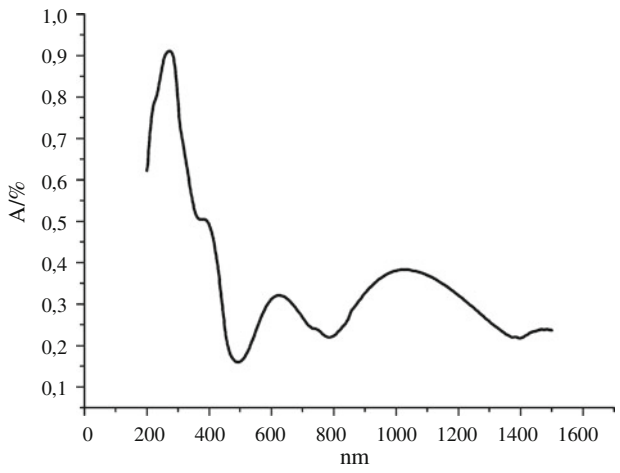

Fig. 2 UV–Vis–NIR spectra for Ni(II) complex

EPR spectra

The Cu(II) complex was examined by EPR spectroscopy and the values for $g_{\|}$ and $g_{\perp}$ were determined for the proper magnetic field (Table 6). The EPR spectra (Fig. 3) and the values of the magnetic field parameters plead for an octahedral symmetry for the Cu(II) complex.

Thermal behaviour of the complexes

The TG/DTA and DSC curves of ligand and complexes are represented in Figs. 4, 5, 6, 7 and 8. The decomposition stages, temperature ranges, heat of decomposition, thermal effects accompanying the changes in the solid complexes on heating, as well as found and calculated weight loss percentages of the complexes are given in Table 7.

The TG/DTA curves show mass loses in three steps, corresponding to the endothermic peaks due to the dehydration and exothermal peaks attributed to the decomposition. The DTG curves show that the thermal decomposition occurs with a large number of consecutive and/or overlapping steps, and through a more complex pathway than that observed from DTA and DSC curves. The area of the endothermic DSC peak corresponds to the melting heat or dehydration, the area of the exothermal peak corresponds to the decomposition heat and the peak temperature corresponds to the melting point, and decomposition temperature, respectively. The decomposition heat was evaluated neglecting the partial superposition of exothermal process.

The thermal TG/DTA and DSC curves of ligand (Fig. 4) shows a melting process, located at 158 °C (peak temperature) on DTA curve and 161 °C on DSC curve, with $\Delta H = 157.69\ Jg^{-1}$ followed by a complex exothermal decomposition. The DSC curve shows two exothermal peaks with maximum temperature at 272 °C, with $\Delta H = -125.42\ Jg^{-1}$ for the first peak and 336 °C, with $\Delta H = -47.21\ Jg^{-1}$, for the second one.

The thermal behaviour of the compounds is depended on the nature of the metal ion. The TG/DTA curve of Cu(II) complex (Fig. 5) shows a mass loss between 50 and 90 °C, corresponding to an endothermic peak at 73 °C on DTA curve, due to dehydration with a loss of $2H_2O$ (Calc. = 4.72%; Exp. = 4.99%). The second step corresponds to the thermal decomposition between 90 and 127 °C with endothermic peak temperature at 117 °C. This step is due to decomposition of one molecule of ligand. The intermediary compound is unstable upon heating and starts to decompose before melting process. This violent decomposition between 127 and 700 °C is due to the removal of SO_3 molecule and decomposition of remaining part of the ligand together with expulsion of a part of the CuO. The overall mass losses are observed to be 72.12%, which is in agreement with the calculated value of 73.73%. On DSC curve, the violent

Table 5 Electronic spectral data and geometries for the ligand and their complexes

Compounds	Frequencies/cm^{-1}	Assignments	$10\Delta q$	B	β	Environment
L	37593	$\pi \rightarrow \pi^*$	–	–	–	–
	32679	$n \rightarrow \pi^*$				
$[CuL_2]SO_4{\cdot}2H_2O$	35211	$\pi \rightarrow \pi^*$	–	–	–	Octahedral
	12722	$z^2 \rightarrow x^2 - y^2$				
$[CoL_2]SO_4{\cdot}2H_2O$	36231	$\pi \rightarrow \pi^*$	6805	613.066	0.631	Octahedral
	19455	$^4T_{1g} \rightarrow {}^4T_{2g}$				
	15337	$^4T_{1g}(F) \rightarrow {}^4A_{2g}$				
	8532	$^4T_{1g} \rightarrow {}^4T_{1g}(P)$				
$[NiL_2]SO_4{\cdot}2H_2O$	36496	$\pi \rightarrow \pi^*$	9708	854.8	0.828	Octahedral
	25906	$^3A_{2g} \rightarrow {}^3T_{2g}$				
	16025	$^3A_{2g} \rightarrow {}^3T_{1g}$				
	9708	$^3A_{2g} \rightarrow {}^3T_{1g}$ (P)				
$[MnL_2]SO_4{\cdot}3H_2O$	34722	$\pi \rightarrow \pi^*$	–	–	–	Octahedral
	30862	CT				

Table 6 EPR data of the Cu(II) complex

Compound	g		H/mT	
	$g_\parallel$	$g_\perp$	$H_\parallel$	$H_\perp$
$[CuL_2]SO_4{\cdot}2H_2O$ (1)	2.3027	2.1011	293.155	321.288

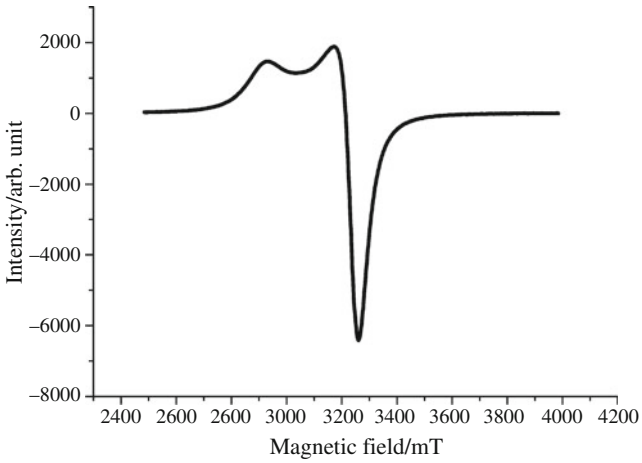

Fig. 3 EPR spectrum of Cu(II) complex at room temperature

decomposition shows a strong exothermal effect with three overlapping peaks, with maximum at 301, 344 and 442 °C. The decomposition heat was evaluated neglecting this partial superposition. The final remaining residue, estimated as cooper oxide, has the observed mass 6.88% as against the calculated value of 10.42%. The total mass loss is in disagreement with TG results, due to the partial expulsion of residue during the violent thermal decomposition. Similar decomposition behaviours are shown in literature [37–39].

The thermal decomposition of the Co(II) complex undergoes in three stages (Fig. 6). The thermal dehydration

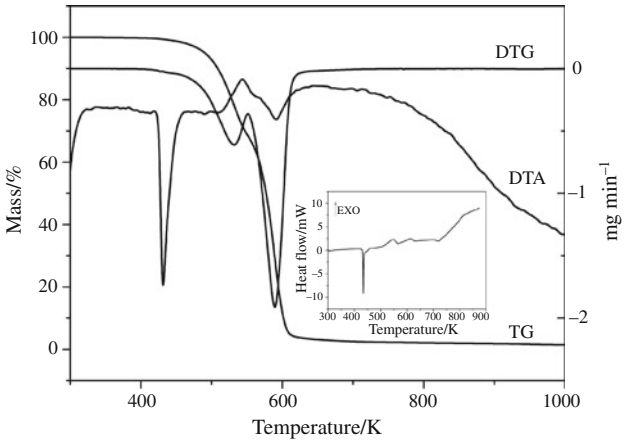

Fig. 4 TG/DTA and DSC curves of L

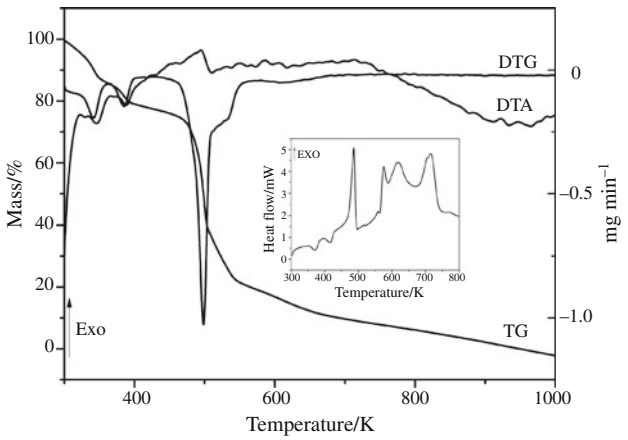

Fig. 5 TG/DTA and DSC curves of $[CuL_2]SO_4{\cdot}2H_2O$

of this complex takes place between 50 and 90 °C, with a mass loss of 4.53% (calc. 4.74%). Two moles of lattice water molecules are removed in this stage of dehydration.

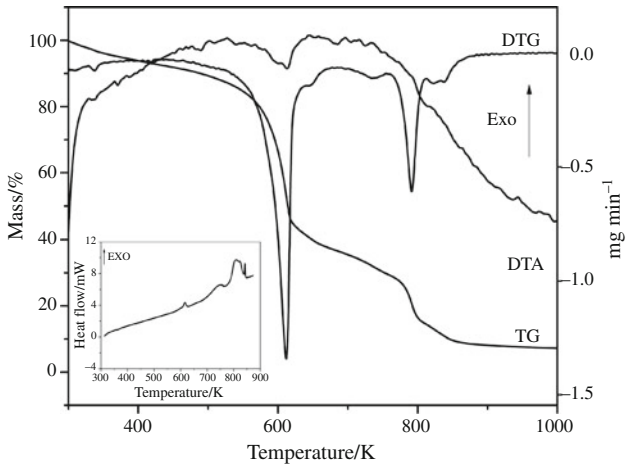

Fig. 6 TG/DTA and DSC curves of $[CoL_2]SO_4{\cdot}2H_2O$

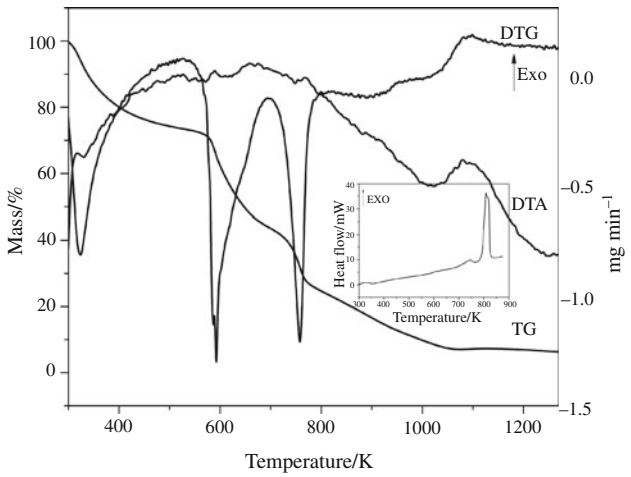

Fig. 7 TG/DTA and DSC curves of $[NiL_2]SO_4{\cdot}2H_2O$

The process is accompanied by endothermic effects at 64 and 94 °C in DTA and DSC curves, respectively. The next step between 90 and 480 °C with peak temperatures at 339 and 343 °C in DTA and DSC curves, respectively, corresponds to the decomposition of one part of the ligand and the removal of one molecule of SO_3. It was observed that the decomposition starts without melting. The observed mass loss for this stage is 65.50% (calc. 66.24%). The third stage, which occurs in the temperature range 480 and 585 °C, corresponds to the decomposition of the remaining part of the ligand. The end product estimated as CoO, has the observed mass of 9.12%, compared with the calculated value of 9.87%.

The thermal decomposition of Ni(II) complex undergo in three stages (Fig. 7). The first DTA peak at 63 °C, in the temperature range 60–80 °C, with the mass loss (exp. 4.61%; calc. 4.74%) corresponds to the loss of two lattice water molecules. This process is further supported by endothermic effect at 78 °C in DSC curve. The second

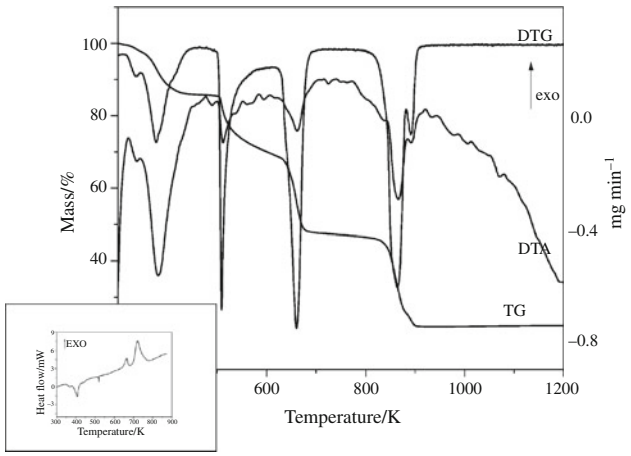

Fig. 8 TG/DTA and DSC curves of $[MnL_2]SO_4{\cdot}3H_2O$

stage occurs in the 80–390 °C temperature range, with the mass loss (49.86%), which is due to the decomposition process (removal of one molecule of SO_3 and one molecule of ligand). This step is accompanied by an exothermal process at 335 °C in DSC curve. With heating, at 5 K min^{-1}, the decomposition of Ni(II) complex starts with melting (the shoulder observed on the endothermic peak at 296 °C in DTG curve) and then decompose. The progressive decrease of TG curve can be observed. An explanation could be that at small heating rates and small quantities of sample, the compound has the sufficient time to absorb heat and to transfer from the solid to the liquid phase by loosening some bond in the crystal lattice [40, 41]. The third stage occurs between 380 and 800 °C, corresponding to the decomposition of the remaining part of the ligand with a mass loss of 38.51% (calc. 39.80%). This process is accompanied by two exothermal effects at 495 and 630 °C in the DTA curve, and 471 and 535 °C in the DSC curve, respectively. The final residue, estimated as free Ni [42–45], has the observed mass 7.02% (calc. 7.77%). In case of Ni(II) complex the percentage of the residue is less that the calculated value corresponding to the full decomposition to the metal so there must be oxide left.

The thermal decomposition of the Mn(II) complex undergoes in three stages (Fig. 8). The thermal dehydration begins at 50 °C and ends at 116 °C with a DTA peak at 108 °C. The observed mass loss (exp. 9.73%; calc. 8.48%) is attributed to the dehydration process. Three moles of lattice water molecules are removed in this stage of dehydration. Because the heat of dehydration calculated from DSC curve have a value of 344.06 Jg^{-1} suggests that the water molecules are strongly kept in the crystal lattice of the complex. The second stage, which occurs in the temperature range 116–403 °C with DTA peak at 389 °C and DSC peak at 391 °C, corresponding to the removal of

Table 7 Thermal analysis data of the complexes

Compounds	TG temperature range/°C	Mass loss/%		DTA peak T/°C	DSC peak T/°C	ΔH/Jg^{-1}	Process	Products
		Exp.	Calcd.					
$[CuL_2]SO_4{\cdot}2H_2O$	50–90	4.99	4.72	73 endo	98 endo	87.82	Loss of lattice water molecule	2 mol H_2O
	90–127	16.01	15.8	117 endo	144 endo	98.39	Removal of one part of ligand	0.4 mol L
	127–700	72.12	73.75	224 exo	215 exo	−703.15	Removal of one molecule of SO_3 and remaining part of ligand, with partial volatilisation of CuO	1 mol SO_3 and 1.4 mol L and partial CuO
				307 exo	301 exo	−396.51		
				431 exo	344 exo	−456.33		
					442 exo	−100581		
	>700	6.88	10.42	–	–	–	Leaving CuO	CuO
$[CoL_2]SO_4{\cdot}2H_2O$	40–90	4.53	4.74	64 endo	94 endo	–	Loss of latice water molecule	2 mol H_2O
	90–480	65.50	66.24	339 exo	343 exo	−70.81	Removal of one molecule of SO_3 and one part of the two molecules of ligand	1 mol SO_3 and 1.4 mol L
	480–585	20.85	21.09	518 exo	535 exo	−1077.09	Removal of remaining part of ligand	0.53 mol L
				549 exo	569 exo	−35.44		
	>585	9.12	9.87	–	–	–	Leaving CoO residue	CoO
$[NiL_2]SO_4{\cdot}2H_2O$	60–80	4.61	4.74	63 endo	78 endo	–	Loss of latice water molecule	2 mol H_2O
	80–390	49.86	50.35	296 endo (melting)	335 exo	−64.60	Removal of one molecule of SO_3 and one molecule of ligand	1 mol SO_3 and 1 mol L
				388 exo				
	390–800	38.51	39.80	495 exo	471 exo	−453.64	Removal of remaining molecule of ligand	1 mol L
				630 exo	535 exo	−3662.14		
	>800	7.02	7.77	–	–	–	Leaving Ni	Ni
$[MnL_2]SO_4{\cdot}3H_2O$	50–116	9.73	8.48	108 endo	134 endo	344.06	Loss of latice water molecule	3 mol H_2O
	116–403	41.65	40.62	239 endo	246 endo (melting)	4.56	Removal of one molecule of SO_3 and part of the two molecules of ligand	1 mol L
				389 exo		−92.05		
					391 exo			
	403–650	27.25	28.00	598 exo	448 exo	−656.93	Removal of another part of molecule of ligand	1 mol SO_3 and mol L
				618 exo				
	>650	21.37	20.11	–	–	–	Leaving MnO and organic residue	MnO and 0.33 mol L

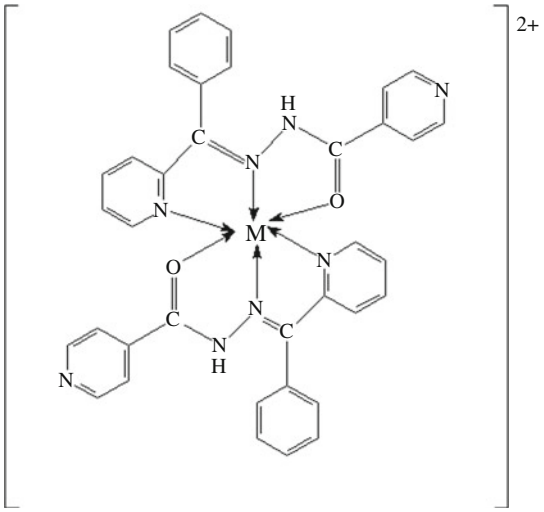

Fig. 9 Structural formula propose for $[ML_2]SO_4{\cdot}xH_2O$ complexes type M = Cu^{2+}, Co^{2+}, Ni^{2+}, $x = 2$; M = Mn^{2+}, $x = 3$

SO_3 molecule and of one part to the ligand. The third stage is related to the decomposition of the remaining part of the ligand in the temperature range of 403–650 °C with two DTA peaks at 598 and 618 °C, respectively. The overall mass loss is observed to be 27.25% (calc. 28.00%). This process is supported by an exothermal peak at 483 °C, in DSC curve. The final residue, estimated as manganese oxide with organic residue [46], has the observed mass 21.37% (calc. 20.11%).

The spectral (IR, electronic and UV–Vis–NIR) and magnetic data together with conductance measurements enable us to predict the possible structural formula for the metal complexes which are also supported by the thermal decomposition studies, as shown in Fig. 9.

Conclusions

Four new complexes of Cu (II), Co (II), Ni (II) and Mn(II) with 2-benzoyl-pyridil-isonicotinoylhydrazone (L) were synthesised and characterised. The structure of the L hydrazone was established by X-ray study on single crystal. The spectroscopic data show that the Schiff base ligand acts as tridentate NNO, being coordinated through the azomethine nitrogen, the pyridine nitrogen and carbonylic oxygen. The thermal decomposition of all studied complexes begins by the release of water, bonded as lattice water. Dehydration begins at 50–100 °C. Next, the anhydrous complexes decompose, in two steps, to the metal oxide. In the case of Ni(II) complex the final residue is estimated as free nickel. The results show that the thermal decomposition of studied complexes is consistent with the elemental and spectral analysis.

Supplementary material

Crystallographic data for the structure in this article have been deposited with the Cambridge Crystallographic Data Centre, CCDC numbers: CCDC 745252. This data can be obtained free of charge at http://www.ccdc.cam.ac.uk/deposit (or from the Cambridge Crystallographic Data Centre, 12, Union Road, Cambridge, CB2 1EZ, UK; Tel: (44) 01223 762910; Fax: (44) 01223 336033; Email: deposit@ccdc.cam.ac.uk).

References

1. Gourbatsis S, Hadjiliadis N, Kalkanis G. The coordination chemistry of N-N′-ethylenebis (2-acetylpyridine imine) and N,N′-ethylenebis (2-benzoylpyridine imine); two potentially tetradentate ligands containing four nitrogen atoms. Trans Met Chem. 1990;15:300–8.
2. Stelzig L, Kotte S and Krebs B. Molybdenum complexes with tridentate NS_2 ligands. Synthesis, crystal structures and spectroscopic properties. J Chem Soc Dalton Trans. 1998;2921–26.
3. Rana A, Dinda R, Sengupta P, Ghosh S, Falvello LR. Synthesis, characterization and crystal structure of cis-dioxomolybdenum (VI) complexes of some potentially pentadentate but functionally tridentate (ONS) donor ligands. Polyhedron. 2002;21:1023–30.
4. Bustos C, Burckhardt O, Schrebler R, Carrillo D, Arif AM, Cowley AH, et al. Synthesis, characterization and electrochemistry of cis-dioxomolybdenum (VI) complexes of Schiff bases derived from carbohydrazide, thiocarbohydrazide, and salicylaldehyde. Inorg Chem. 1990;29:3996–4001.
5. Rana A, Dinda R, Ghosh S, Blake A. A series of new oxomolybdenum (IV) complexes involving some NSO donors as the main ligand frame; the first use of diacetyldihydrazones to stabilize the MoO^{2+} acceptor centre. Polyhedron. 2003;22:3075–82.
6. Costamagna J, Vargas J, Latorre R, Alvarado A, Mena G. Coordination compounds of copper, nickel and iron with Schiff bases derived from hydroxynaphthaldehydes and salicylaldehydes. Coord Chem Rev. 1992;119:67–88.
7. Tandom SS, Chander S, Thompson LK. Liganting properties of tridentate Schiff base ligands, 2[[(2-pyridinylmethyl)imino] methyl]phenol (HSALIMP) and 2-[[[2-(2-pyridinyl)ethyl]imino] methyl]phenol (HSALIEP) with Zn(II), Cd(II), Ni(II) and Mn(III) ions. X-ray crystal structures of the [Zn(SALIEP)(NO3)]2 dimer, [Mn(SALIEP)2](ClO4) and [Zn(AMP)2(NO3)2]. Inorg Chim Acta. 2000;300:683–92.
8. Oshio H, Toriumi MY, Takashima Y. Temperature-dependent crystallographic studies on ferric spin-crossover complexes with different spin-interconversion rates. Inorg Chem. 1991;30:4252–60.
9. Nazir H, Yildiz M, Yilmaz H, Tahir MN, Ulku D. Intramolecular hydrogen bonding and tautomerism in Schiff bases. Structure of N-(2-pyridil)-2-oxo-naphthylidenemethylamine. J Mol Struct. 2000;524:241–50.
10. Jeffery JC, Thornton P, Ward MD. An unusual chainlike tetranuclear manganese (II) complex displaying ferromagnetic exchange. Inorg Chem. 1994;33:3612–5.
11. Dutta SK, Tiekink ERT, Chaudhury M. Mono and dinuclear oxovanadium (IV) compound containing VO(ONS) basic core; synthesis, structure and spectroscopic properties. Polyhedron. 1997;16:1863–71.

12. Scovill JP. A facile synthesis of thiosemicarbazide sand thiosemicarbazone by the transamination of 4-methyl-4-phenyl-3-thiosemicarbazide. Phos Sul Silicon. 1991;60:15–9.
13. Pessoa JC, Tomaz I, Henriques RT. Preparation and characterization of vanadium complexes derived from salicylaldehyde or pyridoxal and sugar derivatives. Inorg Chim Acta. 2003;356:121–32.
14. Ando R, Yagyu T, Maeda M. Characterization of oxovanadium (IV)—Schiff base complexes and those bound or resin, and their use in sulfide oxidation. Inorg Chim Acta. 2004;357:2237–44.
15. Ando R, Mori S, Hayashi M, Yagyu T, Maeda M. Structural characterization of pentadentate salen-type Schiff base complexes of oxovanadium (IV) and their use in sulfide oxidation. Inorg Chim Acta. 2004;357:1177–84.
16. Pelagatti P, Carcelli M, Pelizzi C, Costa M. Polymerization of phenylacetylene in water catalyzed by Pd(NN′O)Cl complexes. Inorg Chim Acta. 2003;342:323–6.
17. Jang YJ, Lee U, Koo BK. Synthesis and crystal structures of Mn(II), Co(II), Ni(II), Cu(II) and Zn(II) metal complexes with NNO functionalized ligands. Bull Korean Chem Soc. 2005;26(6):925–9.
18. Konstantinovi SS, Radovanovi BS, Krklješ A. Thermal behaviour of Co(II), Ni(II), Cu(II), Zn(II), Hg(II) and Pd(II) complexes with isatin-β-thiosemicarbazone. J Thermal Anal Calorim. 2007;90(2):525–31.
19. Dogan F, Ulusoy M, Öztürk ÖF, Kaya I, Salih B. N,N′-BIS(3,5-DI-t-butylsalicylideneimine) propanediamine and its some tetradentate Schiff base complexes synthesis, characterization and thermal study. J Thermal Anal Calorim. 2008. doi:10.1007/S10973-008-9099-7.
20. Köse DA, Gökçe G, Gökçe S, Uzun I. Bis(n,n-diethylnicotinamide) p-chlorobenzoate complexes of Ni(II), Zn(II) and Cd(II) Synthesis and characterization. J Thermal Anal Calorim. 2009;95(1):247–51.
21. Kriza A, Tatucu M, Stanica N, Anoaica PG. Coordination compounds of several transition metals with phenyl-2-pyrydylketone. Rev Chim (Bucharest). 2008;59(5):505–10.
22. Kriza A, Tatucu M, Maxim C, Stanica N. Synthesis and structural studies of Co(II), Ni(II) and Cd(II) complexes with 2-acetylpyridine. J Coord Chem. 2009;62:106–11.
23. Stoe&Cie. X-AREA (version1.18). Darmstadt, Germany: Stoe&Cie; 2002.
24. Sheldrick GM. SHELXS-97, a program for the solution of crystal structures. Germany: University of Gottingen; 1997.
25. Sheldrick GM. SHELXL-97, a program for the solution of crystal structures. Germany: University of Gottingen; 1997.
26. Geary WJ. The use of conductivity measurements in organic solvents for the characterization of coordination compounds. Coord Chem Rev. 1971;7:81–122.
27. Mojumdar SC, Simon P, Krutosikova A. [1]Benzofuro[3,2-c]pyridine synthesis and coordination reactions. J Thermal Anal Calorim. 2009;96:103–9.
28. Kriza A, Parnau C, Popa N. Complexes combination with 1-H-indol-2,3-dione. Rev Chim (Bucharest). 2001;52(6):346–8.
29. Nakamoto K. Infrared Spectra of Inorganic and Coordination Compounds. 2nd ed. New York, NY: Wiley; 1970.
30. Serna EZ, Urtiaga KM, Barandika MG, Cortes R, Martin S, Lezama L, et al. Dicubane-like tetrameric cobalt(II)—pseudohalide ferromagnetic clusters. Inorg Chem. 2001;40:4550–5.
31. Serna EZ, Urtiaga KM, Barandika MG, Cortes R, Lezama L, Arriotua MI, Rojo T. Investigation of the Cu^{II}/NCS^{-}/dpk reaction system in CH_3OH [dpk = Di(2-pyrydil)ketone. Eur J Inorg Chem 2001:(3);865–72.
32. Kahn O. Molecular magnetism. New York: VCH; 1993.
33. Agarwal RK, Sharma D, Shing L, Agarwal H. Synthesis, biological, spectral and thermal investigations of cobalt(II) and nickel(II) complexes of N-isonicotinamido-2,4-dichlorobenzalaldimine. Bioinorg Chem Appl. 2006. doi:10.1155/BCA/2006/29234.
34. Aurkie R, Banerjee S, Sen S, Butcher RJ, Rosair GM, Garland MT, et al. Two Zn(II) and one Mn(II) complexes using two different hydrazone ligands: spectroscopic studies and structural aspects. Struct Chem. 2008;19(2):209–17.
35. Lever ABP. Inorganic electronic spectroscopy. Amsterdam, The Netherlands: Elsevier; 1984.
36. König E. The nephelauxetic effect calculation, accuracy of the interelectronic repulsion parameters I. Cubic high-spin d2, d3, d7 and d8 systems. Struct Bonding. 1971;9:175–212.
37. Bannach G, Siqueira AB, Ionashiro EY, Rodrigues EC, Ionashiro M. Solid-state compounds of 2-chlorobenzylidenepyruvate with some bivalent metal ions synthesis, characterization and thermal behaviour. J Thermal Anal Calorim. 2007;90(3):873–9.
38. Ferenc W, Walków-Dziewulska A. Thermal and spectral features of yttrium and heavy lanthanide complexes with 2,4 dimethoxybenzoic acid. J Thermal Anal Calorim. 2001;63:865–77.
39. Kriza A, Dianu ML, Andronescu C, Rogozea AE, Musuc AM. Synthesis, spectral and thermal studies of new copper (II) complexes with 1,2-di(imino-2-aminomethylpyridil)ethane. J Therm Anal Calorim. 2009. doi:10.1007/s10973-009-0425-5.
40. Lalia-Kantouri M. Factors influencing the thermal decomposition of transition metal complexes with 2-oh-aryloximes under nitrogen. J Thermal Anal Calorim. 2005;82(3):791–6.
41. Oancea D, Musuc AM, Razus D. Study of exothermal decomposition of some nitrophenylhydrazine derivatives using differential scanning calorimetry method. Rev Chim (Bucharest). 2003;54(4):331–4.
42. Souaya ER, Ismail EH, Mohamed AA, Milad NE. Preparation, characterization and thermal studies of some transition metal ternary complexes. J Thermal Anal Calorim. 2009;95(1):253–8.
43. Modi CK, Patel MN. Synthetic, spectroscopic and thermal aspects of some heterochelates. J Thermal Anal Calorim. 2008;94(1):247–55.
44. Pansuriya PB, Dhandhukia P, Thakkar V, Patel MN. Dicoumarol complexes of Cu(II), Fe(II) and Fe(III): preparation, characterization, in vitro antibacterial and DNA binding activity. J Enzym Inhib Med Chem. 2007;22:477–87.
45. El-Metwally NM, Gabr IM, Shallaby AM, El-Asmy AA. Synthesis and spectroscopic characterization of new mono and binuclear complexes of some NH(1) thiosemicarbazides. J Coord Chem. 2005;58:1145–59.
46. Czakis-Sulikowska D, Radwañska-Doczekalska J, Markiewicz M, Pietrzak M. Thermal characterization of new complexes of Zn(II) and Cd(II) with some bipyridine isomers and propionates. J Thermal Anal Calorim. 2008;93:789–94.